LBNL-44167
DA-409

Design and Evaluation of Daylighting Applications of Holographic Glazings

Final Report prepared for
Physical Optics Corporation under
Contract Agreement Number BG-95037

K. Papamichael, C. Ehrlich and G. Ward
Building Technologies Program
Environmental Energy Technologies Division
University of California
1 Cyclotron Road
Berkeley, CA 94720

December 1996

This work was supported by the Physical Optics Corporation through the U.S. Department of Energy under Contract No. DE-AC03-76SF00098.

Design and Evaluation of Daylighting Applications of Holographic Glazings

Final Report prepared for
Physical Optics Corporation under
Contract Agreement Number BG-95037

K. Papamichael, C. Ehrlich and G. Ward

Introduction

This is the final report on a study performed by Lawrence Berkeley National Laboratory for Physical Optics Corporation, under Contact Number Agreement BG-95037. The main purpose of this study was to assist Physical Optics Corporation with the design and evaluation of holographic glazings for daylighting applications.

Background

When combined with appropriate electric lighting dimming controls, the use of daylight for ambient and task illumination can significantly reduce energy requirements in commercial buildings. While skylights can effectively illuminate any part of one-story buildings, conventional side windows can illuminate only a 15 ft - 20 ft (4.6 m - 6.1 m) depth of the building perimeter. Even so, the overall efficacy of daylight is limited, because side windows produce uneven distributions of daylight. Achieving adequate illumination at distances further away from the window results in excessive illumination near the window, which increases cooling loads from the associated solar heat gain. As a result, the use of larger apertures and/or higher transmittance glazings, to introduce daylight deeper than 15 ft - 20 ft (4.6 m - 6.1 m), may prove ineffective with respect to saving energy, because cooling load penalties may exceed the electric lighting savings.

The need for more uniform distribution of daylight admitted through side windows has stimulated significant research and development efforts in new fenestration designs and glazing technologies. Many of these approaches, including holographic glazings, rely on the common strategy of redirecting sunlight and reflecting it off the ceiling towards the back of the room. Prior studies on the daylight and energy performance of holographic glazings have been disappointing, however inconclusive because of poor hologram quality, low diffraction efficiency and inadequate hologram design and building application considerations [Papamichael et al 1994].

Contractual Agreement

In the 1993-94 time frame, Physical Optics Corporation (POC) initiated a two-year effort to develop marketable holographic glazings for daylighting applications, based on multi-function holographic structures that, in addition to redirecting light at high diffraction efficiencies, offer spectral selectivity and diffuse shaping of the diffracted radiation. At that time, POC requested the collaboration of the Building Technologies Program (BTP) at Lawrence Berkeley National Laboratory (LBNL). BTP had a long history of daylighting research and development, which included a previous study on the daylight and energy performance of holographic glazings [Papamichael et al 1994].

Scope and Objectives

According to the contractual agreement, BTP would develop a computer model of the POC holographic structures and then simulate the performance of alternative designs using the RADIANCE lighting and rendering computer program [Ward 1990]. The RADIANCE model would then be used to evaluate the daylight performance of alternative designs of holographic glazings in a prototypical office space. The simulation process would be validated against actual photometric measurements of holographic glazing samples developed by POC. The results would be used to evaluate the potential for increased electric lighting savings through increased daylight illuminance levels at distances more than 15 ft - 20 ft (4.6 m - 6.1 m) from the window wall.

Algorithmic Evaluation

In collaboration with POC, LBNL developed algorithms to model the behavior of holographic glazings. These algorithms were coded into subroutines that were used with the RADIANCE lighting and rendering computer program to simulate the daylight performance of holographic glazings when applied to side apertures in prototypical office spaces.

Diffraction Modeling

The modeling of the radiative behavior of holographic glazings was based on the equations provided to LBNL by POC. These equations are used to compute diffracted direction and efficiency, based on a given incident direction of radiation. The initial sets of equations provided by POC were not compatible with the way that RADIANCE computes light propagation. The equations were approximating diffraction direction, while RADIANCE needed exact directions of each ray in order to find a light source as small (in terms of angular size) as the sun. To overcome this limitation and to avoid the cost of numerically averaging over many incident polarizations, POC developed a new set of equations providing a closed-form solution to the randomly polarized average.

Using the second set of equations, LBNL developed two versions of the basic hologram model. In the first version, one enters the exact wavelength of light to simulate, and the computation is carried out at that wavelength only. In the second version, a range of wavelengths is averaged to get a better (though slower) approximation to the continuous spectrum of the solar radiation.

Daylighting Modeling

RADIANCE employs a variant of ray tracing, where light is followed backwards from the point of measurement (usually a camera) into a scene and to the light sources. Because of this, re-directions such as diffraction by holographic glazings must be treated specially. In a preprocessing step, RADIANCE identifies all redirecting surfaces and the light sources that may be redirected by them. The provided formulas for new ray directions and coefficients are then used to determine general behavior for each surface, and a set of virtual light sources is created. In the case of our holographic glazing, one new sun is created for a total of two light sources. One is in the same position as the original sun, representing the transmitted component, and one is in the position of the diffracted component (Figure 1).

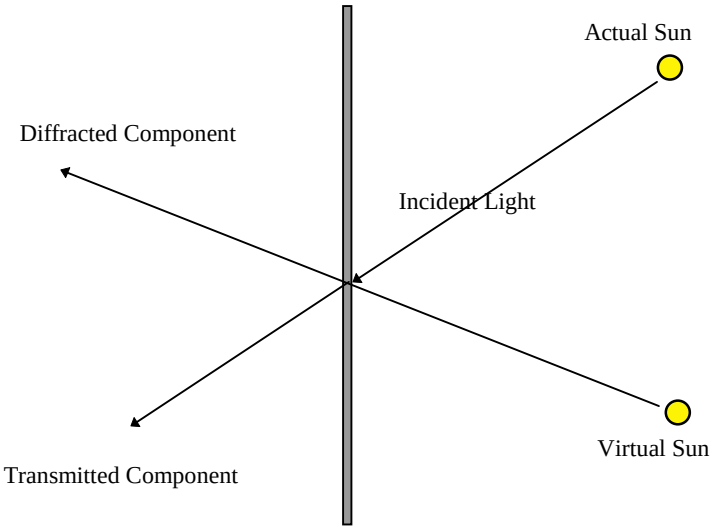

Figure 1. RADIANCE preprocessing step establishes locations for virtual sources needed to compute diffracted radiation during simulation.

Because the preprocessing step computes light from the source perspective, it relies on correct reciprocal behavior in the equations in order to then find the source again from the other side during the actual simulation. Because the formulas used are exact only at the Bragg condition, it was necessary to fudge the expected direction in order to find the sun during the simulation. This should result in no greater error than using the direction computed with the approximate formulas, since the approximate formulas determine the direction, but from the other side of the glazing in the preprocessing stage.

Image Generation

RADIANCE can generate photo-accurate images of the simulated environment. This capability was used to verify the validity of the holographic simulation runs. Images were generated initially by combining the results of independent simulations performed at three averaged wavebands for red, green and blue channels, with 25 samples each, for a total of 75 visible wavelengths (Figure 2).

Photometric Evaluation

Parallel to the development of the algorithms for the computer-based simulations, LBNL performed photometric evaluations of a 2" by 4" holographic glazing sample provided by POC. The sample was a more complex hologram than the hologram for which algorithms were developed, because the sample included both diffracting and diffusing hologram layers.

Experimental Setup

The complex sample was tested with a tabletop goniometer using both white light and HeNe laser light (Figure 3). The goniometer assembled by LBNL included a BaO-coated integrating sphere mounted on an adjustable arm, which allowed the port of the sphere to be adjusted to trap either the diffracted, specular, or total transmitted light. The purpose for the goniometer tests was to measure the efficiency and design diffraction and acceptance (incident) angles of the holographic sample in order to calibrate the RADIANCE holographic rendering algorithms.

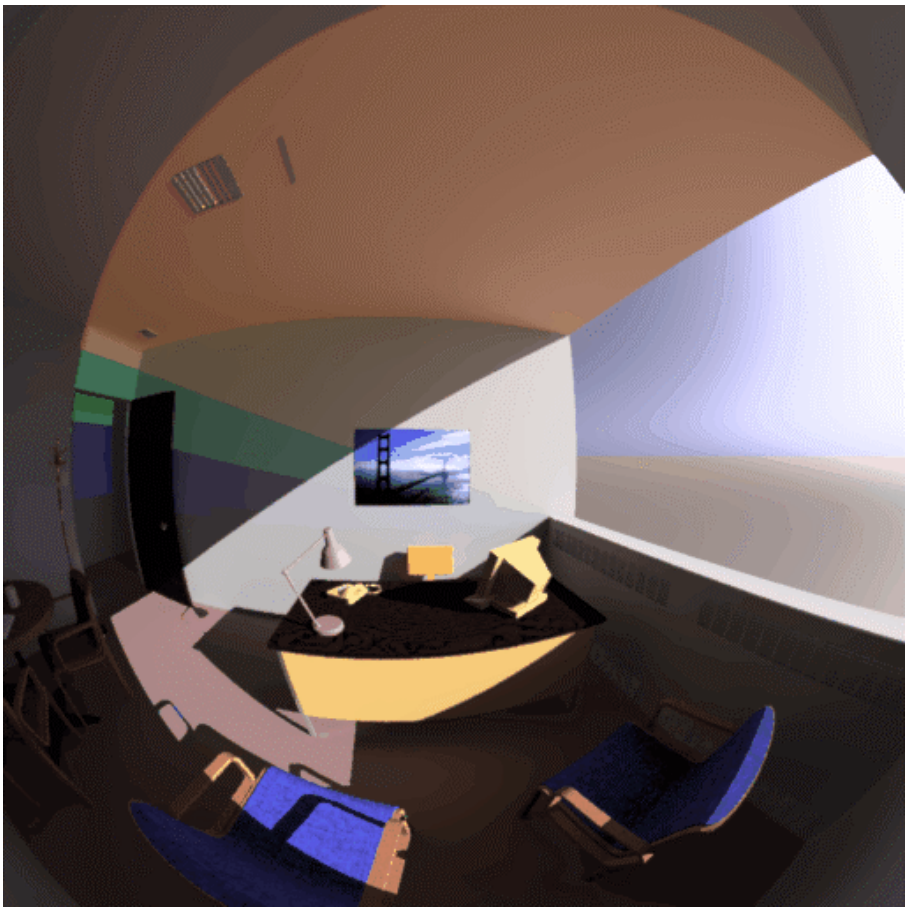

Figure 2. Visual simulation of simple hologram, showing colored diffraction.

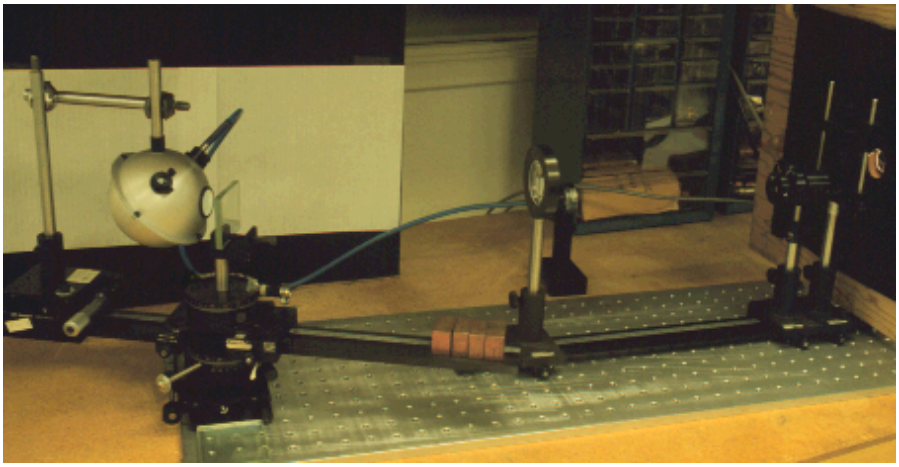

Figure 3. Tabletop goniometer setup with integrating sphere, collimating lenses, fiber-optic cable and mounted sample.

The hemispherical efficiency at the hologram's design diffraction angle was measured for 5 incident angles of light including 0° (normal), 22.5°, 45°, 50°, and 67.5° (Figure 4). A distinct quadrilateral symmetry of the output distribution was observed and the sample was oriented such that incident light would be diffracted in the appropriate direction.

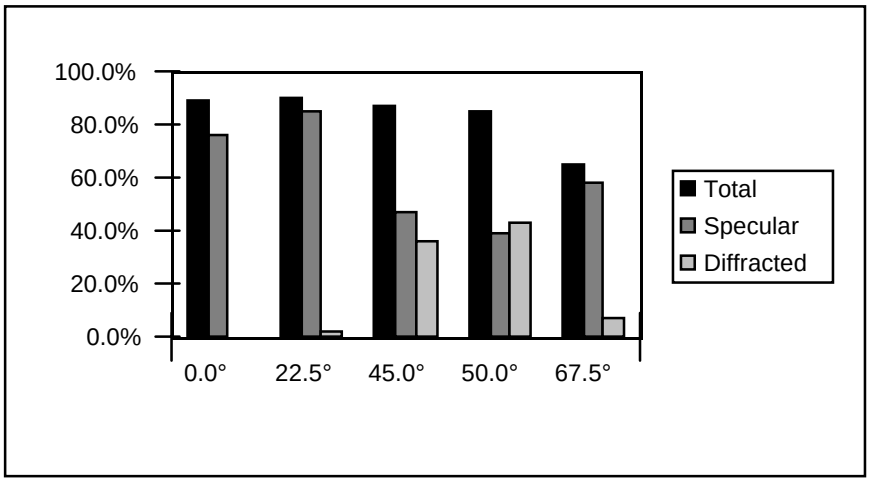

Figure 4. Efficiency of the POC diffracting and diffusing holographic sample at 5 incident angles of collimated white light at incident plane.

Analysis of Measurements

Analyses of white light measurements show that the "acceptance angle" of the sample was approximately 50 degrees. Acceptance angle is defined as the angle at which the hologram was designed to accept light for optimum diffraction efficiency. The sample's "diffraction angle" was more difficult to ascertain because of the diffusing hologram's effect. Diffraction angle is defined as the angle at which the hologram is designed to most efficiently diffract light. For all incident angles, the diffraction hologram very thoroughly mixed the output distribution, clear evidence that the diffusing hologram in the provided sample was working well. The maximum white-light diffusing angle was measured at 55.7 degrees. A rainbow effect was still clearly visible.

To further refine the measurement of the design diffraction angle, a HeNe laser was used. Unfortunately, no single output diffraction angle was observed again because of the diffusing hologram's effect. The peak of the HeNe laser diffracted output was measured at 57 degrees for a peak incident angle of 53 degrees. Since this was close to our measured white light incident angle, the diffraction angle for green light was assumed to be the white light value of 55.7 degrees.

Since the holographic glazing sample used for the measurements was more complex than the holographic glazings described by the equations provided by POC, there was no way to definitively verify the algorithmic modeling. Using the efficiency parameters that we could measure, we compared them to the calculated efficiency and found them to be similar enough to bolster confidence in the simulation.

Parametric Simulations

A simple room was used for a parametric simulation of the application of holographic glazing for a prototypical perimeter glazing office (Figure 5).

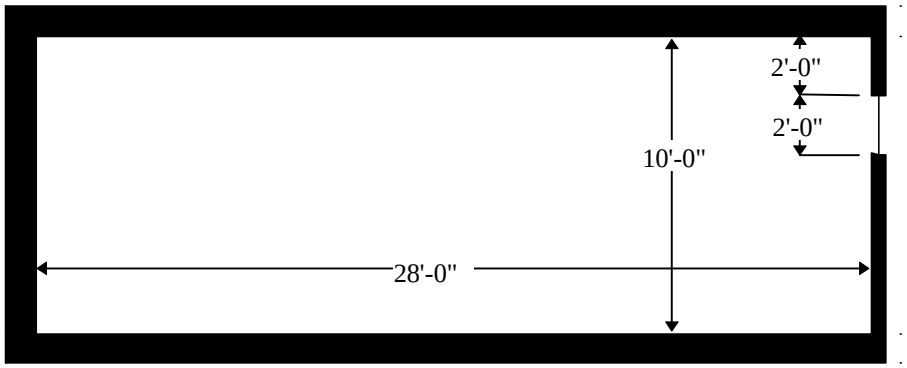

Figure 5. Section through prototypical Clerestory Office.

The prototypical clerestory office was modeled in RADIANCE. The office has a ten-foot high ceiling and is 20 feet wide by 28 feet deep with a two-foot tall clerestory light at the south end of the room spanning from 6 feet to 8 feet above the floor. The average diffuse reflectance of the walls was 43.5%; the ceiling was 76.3% and the floor was 21%. The office is assumed to be located in Berkeley, California with a latitude of 37.8° and a longitude of 122°. The sky condition for the parametric runs were CIE clear skies with direct solar radiation. Simulations were conducted at noon on December 21, February 11, March 21, May 11 and June 21.

The ideal application of this holographic glazing was envisioned to be with clerestory lights above standard perimeter glazing. In our judgment, the haze and rainbow banding effects noticed in the POC samples would be unacceptable as vision glass in most perimeter glazing office installations. Furthermore, narrower strips of holographic glazing are presumed to be less costly to manufacture. The office simulation was modeled with only a clerestory light (no vision glass below) in order to isolate the potential contribution to the light levels from the band of clerestory holographic glazing.

An initial set of simulations was carried our for clear glass, to establish a “base case” for comparison purposes (Figure 6). All holographic glazing runs were then compared to the “base case.”

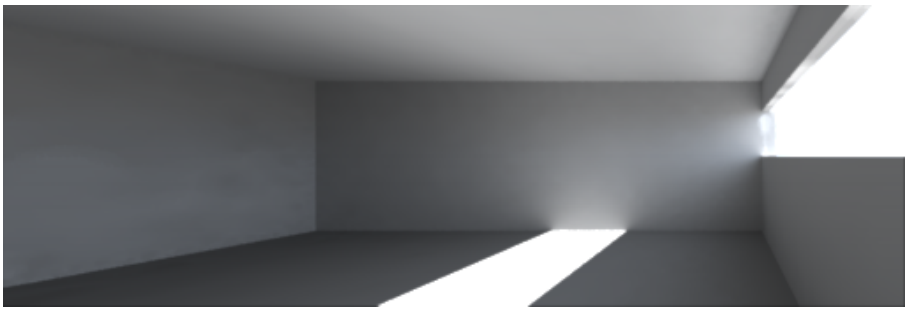

Figure 6. Prototypical Clerestory Office simulation rendered with clear glass.

To minimize the calculation times for the parametric simulation a sampling of 25 wavelengths of light around green was used as an approximation for the entire visible spectrum. Low-resolution renderings were performed to verify that the results pass a basic visual validity check. The first simulation used a hologram that matched the sample hologram provided by POC in order to calibrate the RADIANCE rendering algorithms.

As shown in Figure 7, the provided sample is not ideal for use as a daylighting device because it does not diffract light towards the back of the office. However, the hologram design efficiency was close to our measured efficiency for direct sun at its optimum design conditions.

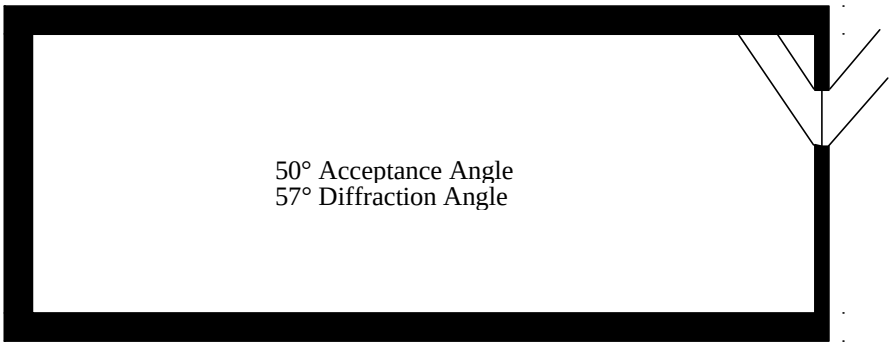

Figure 7. The design of the provided sample shown relative to the prototypical office section.

At angles other than the design conditions, the hologram's efficiency dropped rapidly and had undesirable side effects. Figure 8 shows the conditions for Noon on June 21. Notice the band of diffracted light spanning the back wall of the office. Only about 5% of the incident light was being directed to the back wall of the office. The diffracted direction was close to horizontal (a potential glare problem) because the incident light was greater (higher in the sky) than the design acceptance angle. This causes the diffracted angle to follow as if rotating on an axis parallel to the pane of glass.

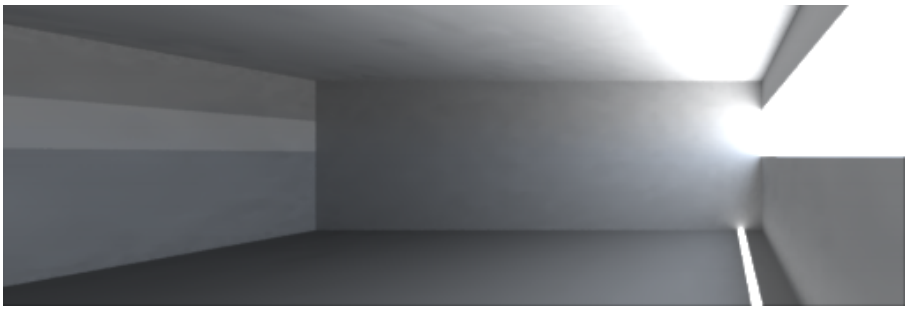

Figure 8. Prototypical Clerestory Office simulation using holographic glazing with 50° acceptance and 55.7° diffraction angles for Noon on June 21 (direct solar radiation is at 67.6°).

Holographic Glazing Design

After the initial simulation of the holographic glazing design that matched the sample provided by POC, a new design was considered for the parametric analyses using formulas derived from the holographic glazing algorithms provided by POC. The design algorithms are listed in the Appendix.

First Design

The shape of the prototypical office was studied to determine a more appropriate design for the holographic acceptance and diffraction angles. The first hologram was designed to aim the green wavelength of light at the center of the ceiling. We chose not to aim for the back of the office because of our concern that shallower diffraction angles would be less efficient and could cause light to be diffracted at near horizontal angles causing potential glare problems. We chose to optimize the acceptance angle for June 21st to maximize our potential improvement in the summer months when non-diffracted direct sun is limited to the front of the office (Figure 9).

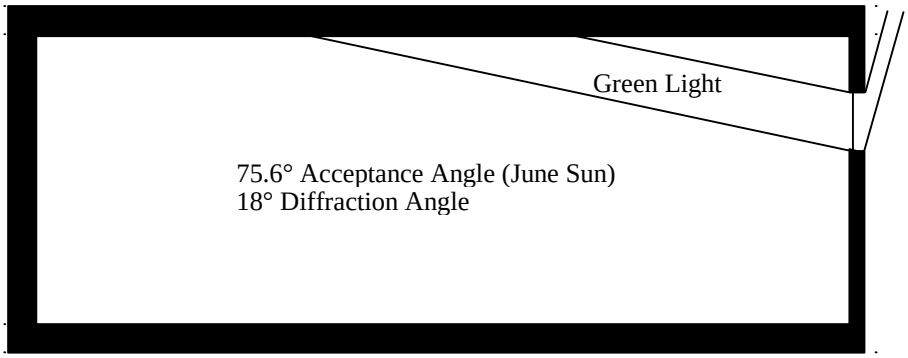

Figure 9. Section of prototypical office showing incident and diffracted design angles for .555 micron direct solar radiation at Noon on June 21st.

Using the design algorithms described in the Appendix, a simulation of the distribution of natural daylight with direct sun and diffuse sky components included was performed. In all cases, the holographic glazing was compared to an identical office with clear glazing at the same time and month. The low-resolution renderings used to partially verify the simulations are shown in Figure 10 for clear glazing and holographic glazing with 75.6° acceptance and 18° diffraction angles. A plot of the illuminance values at a height of 30 inches from the floor shows nominal improvement in the distribution of light in the office (Figure 11).

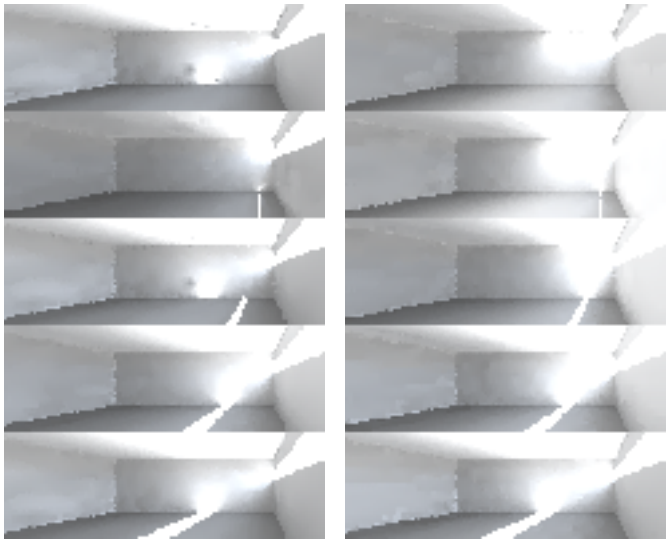

Figure 10. Clear and holographic glazing with 75.6° acceptance (June 21st) and 18° diffraction angles at solar noon on June 21, May 11th, March 21st, February 11th, and December 21st (top to bottom).

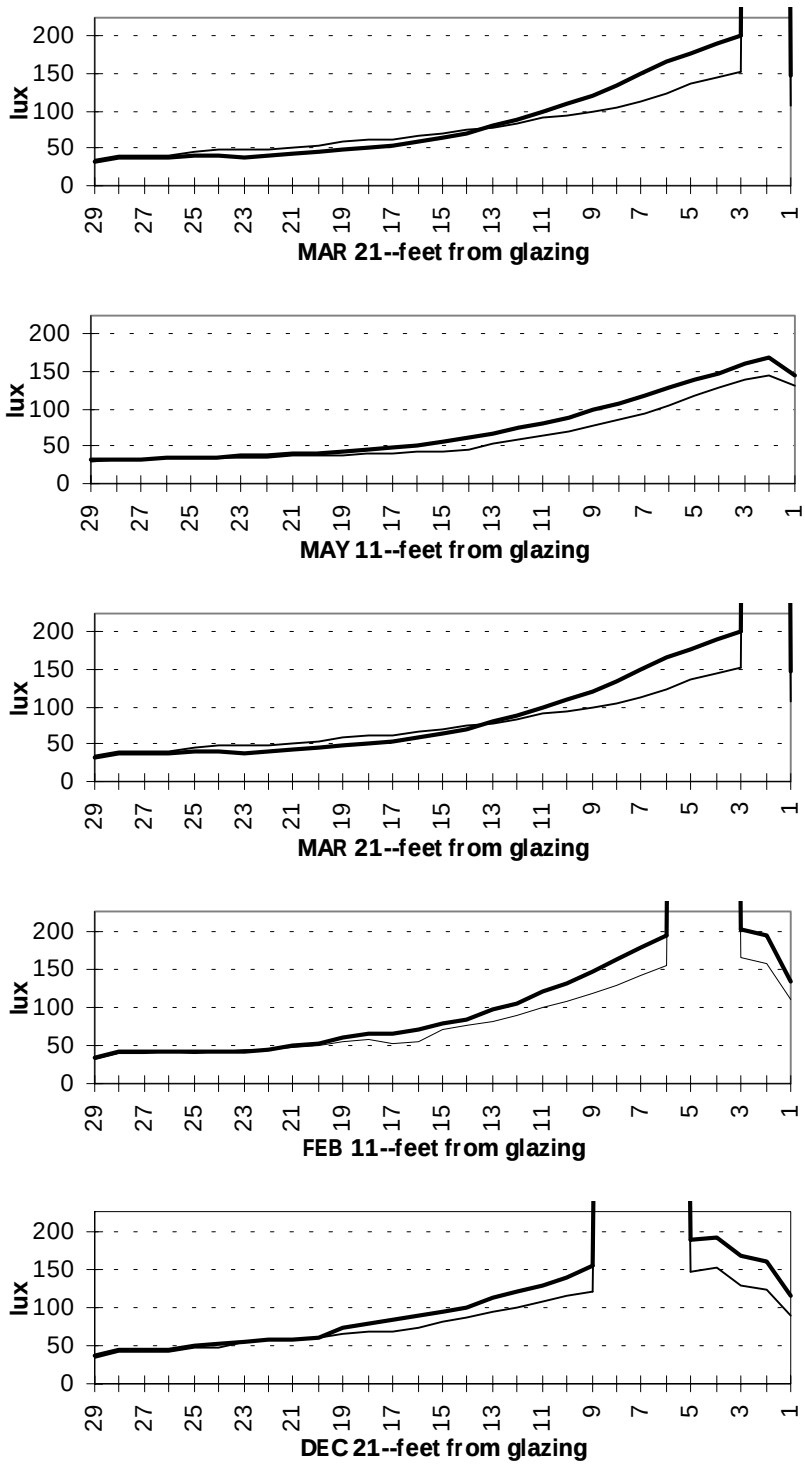

Figure 11. Illuminance distribution at 30 inches above the floor with holographic glazing with 75.6° acceptance and 18° diffraction angles (bold line) versus clear glazing (thin line).

Second Design

Unable to find significant improvements in the distribution of natural daylight with the first design, the analyses continued with a hologram design that was optimized for solar noon on March 21st as shown in figure 12.

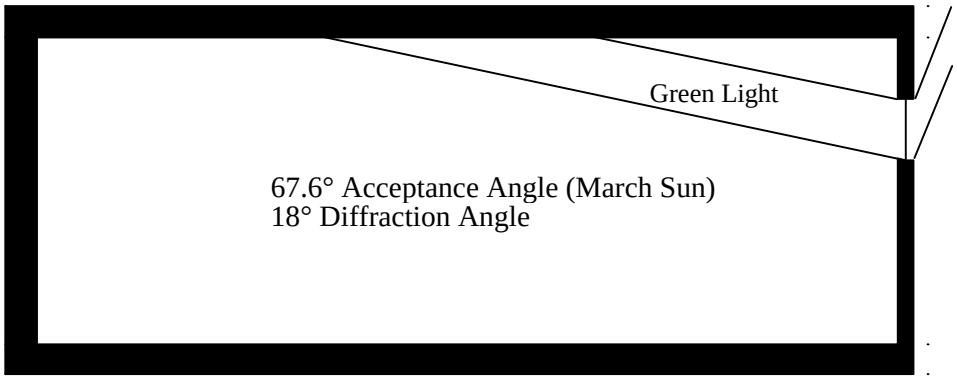

Figure 12. Section of prototypical office showing incident and diffracted design angles for green (.555 micron) direct solar radiation at Noon on March 21st.

Figure 13 compares the office with clear glazing to the office with holographic glazing with 67.6° acceptance and 18° diffraction angles.

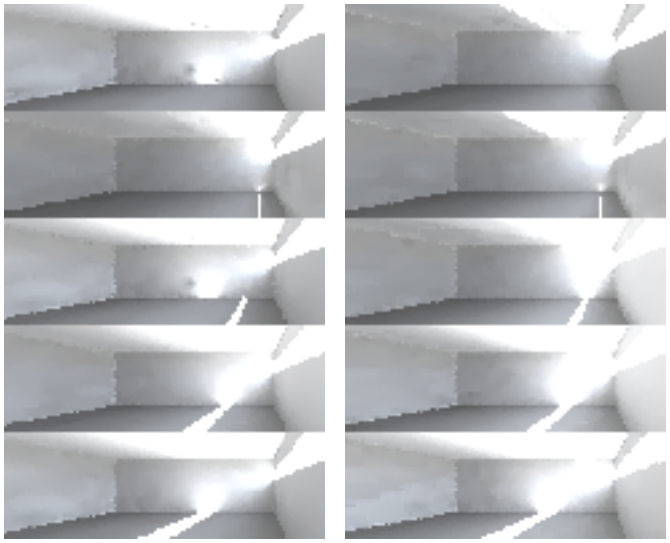

Figure 13. Clear and holographic glazing with 67.6° acceptance (March 21st) and 18° diffraction angles at solar noon on June 21, May 11th, March 21st, February 11th, and December 21st (top to bottom).

As shown in Figure 14, this design showed a measurable and significant improvement in the performance in June and May. Yet, the performance in December through March is still nominal. The added daylight performance is still limited to the front of the office.

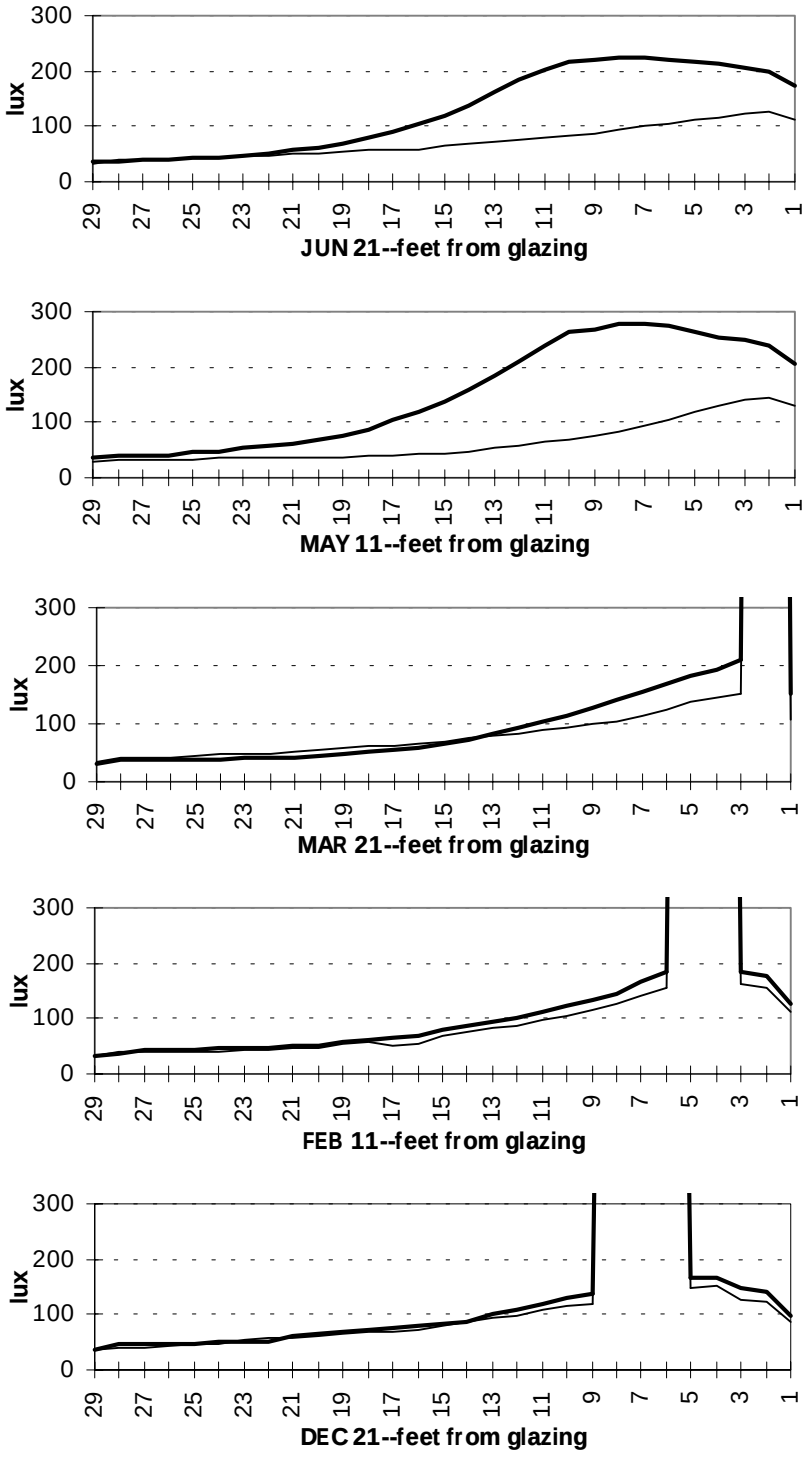

Figure 14. Illuminance distribution in room with holographic glazing with 67.6° acceptance (March 21st) and 18° diffraction angles (bold line) versus clear glazing (thin line).

Third Design

Seeing the small difference at the back of the room for the first and second designs, we designed a hologram which aims the diffracted light towards the back of the room at a diffraction angle of 8 degrees with an acceptance angle of 75.6 degrees (Noon, June 21st), as shown in Figure 15.

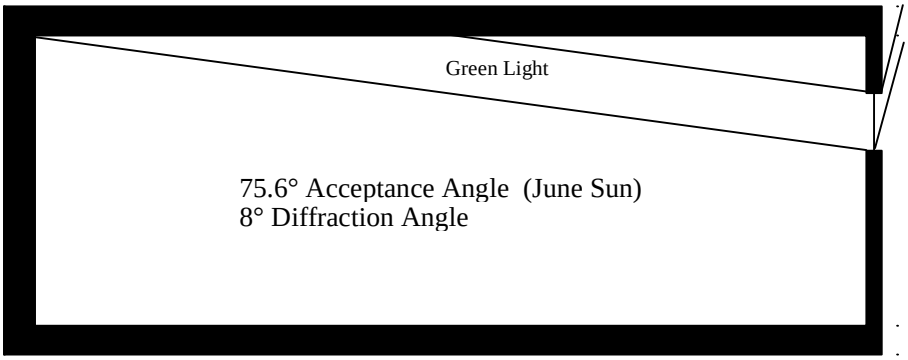

Figure 15. Section of prototypical office showing incident and diffracted design angles for green light (.555 micron) direct solar radiation at Noon on March 21st.

Figure 16 compares the office with clear glazing to the office with holographic glazing with 67.6° acceptance and 18° diffraction angles. Even through light is diffracted towards the back part of the ceiling, especially in June and May, it is not enough to make a significant difference on the work-plane illuminance levels, as shown in figure 17.

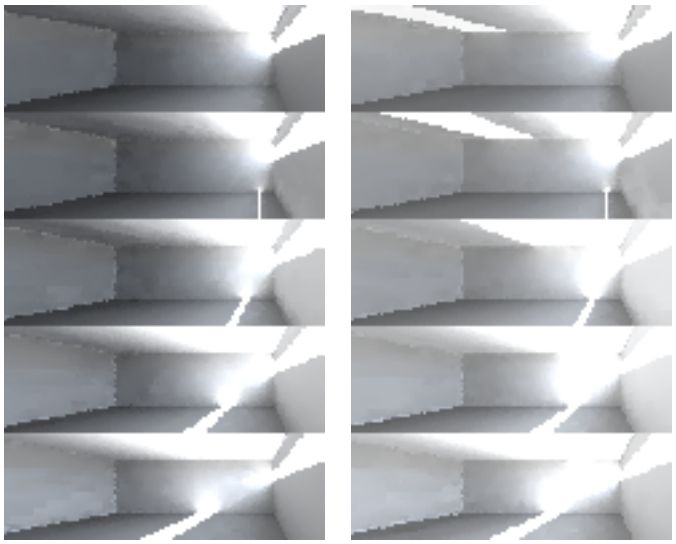

Figure 16. Clear and holographic glazing with 75.6° acceptance (June 21st) and 8° diffraction angles at solar noon on June 21, May 11th, March 21st, February 11th, and December 21st (top to bottom). Notice the band of light across the ceiling.

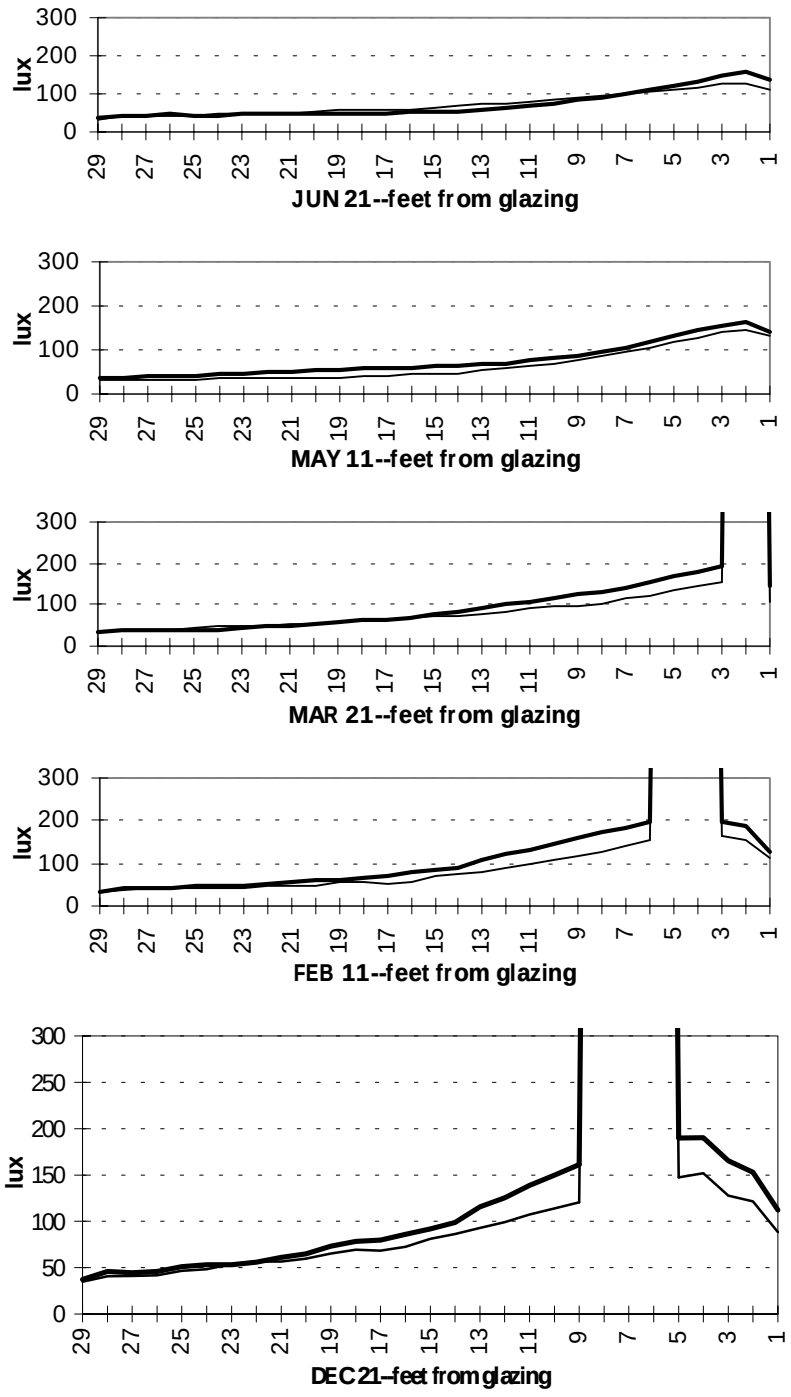

Figure 17. Illuminance distribution in room with holographic glazing with 75.6° acceptance (June 21st) and 8° diffraction angles (bold line) versus clear glazing (thin line).

Conclusions

Based on the results of our analyses, we conclude that this type of holographic glazing technology only nominally increases the illuminance levels at the back of the office. Since the performance was so low even for the design conditions, no runs were made for oblique sun angles, because the performance is expected to be even worse.

Based on the algorithms provided by POC, the primary limitation of this hologram technology is that it has a very narrow band of efficiency limited by acceptance angle and design wavelength. The steeper the acceptance angle and the shallower the diffraction angle, the less efficient the hologram becomes. Unfortunately, these are the desired angles for redirecting sunlight at the back of the room through side window applications.

Acknowledgment

This work was supported by the Physical Optics Corporation through the U.S. Department of Energy under Contract No. DE-AC03-76SF00098.

References

K.M. Papamichael, L..O. Beltrán, R. Furler, E.S. Lee, S. Selkowitz and M. Rubin. "Simulating the Energy Performance of Prototype Holographic Glazings." *Proceedings of the SPIE's 13th International Symposium on Optical Materials Technology for Energy Efficiency and Solar Energy Conversion*, Freiburg, Germany, April 18-22, 1994.

G.J. Ward. "Visualization." *Lighting Design + Application*, Vol. 20, No. 6, pp. 4-20, 1990.

Appendix: Computer Code

Several new subroutines were developed for the modeling of the holographic glazings using the RADIANCE lighting simulation and rendering computer program. These are listed below.

diffract.cal

This subroutine was used to compute the diffracted direction and efficiency (as well as the transmitted efficiency) using the formulas provided by POC, plus the standard Fresnel equations for the glass-air interface. The computations are for a single, discrete wavelength. The subroutine was checked against example computations provided by POC.

```
{
    Diffraction equation for grating without diffuser.

    Grating surface is in the X-Y plane, with grating aligned
    along the Y axis (i.e. rays are bent in X by grating).

    Taken from formulas provided by Physical Optics Corporation.
    Contact Indra Tengara (310) 320-3088 or (909) 396-0333.

    Grating-related input parameters:

    A1      - average index of refraction
    A2, A3, A4  - X, Y, Z of grating vector (1/microns)
              (X and Z must be positive, Y always zero)
    A5      - thickness of grating (microns)
    A6      - index modulation magnitude
    A7      - sample wavelength (microns)

    Computed values:

    dc      - diffracted component coefficient
    ddx, ddy, ddz   - diffracted component direction
    tc      - transmitted component coefficient
    tdx, tdy, tdz   - transmitted component direction
}
WL = arg(7);        { sample wavelength (microns) }
WN = 2*PI/WL;       { wave number in vacuum (1/microns) }

            { hologram-specific parameters }
n_avg = arg(1);         { average index of refraction }
Kx = arg(2);            { X component of grating vector (1/microns) }
Ky {= arg(3)} : 0;      { Y component of grating vector (always zero) }
Kz = arg(4);            { Z component of grating vector }
t_h = arg(5);           { grating thickness (microns) }
n_1 = arg(6);           { index modulation }

            { Fresnel reflection coefficients }
dot = abs(Dz);
C2 = sqrt(1 - (1-dot*dot)/(n_avg*n_avg));
F2_perp = sq((1/dot - n_avg/C2)/(1/dot + n_avg/C2));
F2_par = sq((dot - n_avg*C2)/(dot + n_avg*C2));
refl = .5 * (F2_perp + F2_par);
trans = 1 - refl;

            { Wave variables and diffracted direction }
K = sqrt(Kx*Kx + Ky*Ky + Kz*Kz);
beta = WN*n_avg;
chi = WN/2*n_1;
k_dx = beta*Dx - Kx; k_dy = beta*Dy - Ky; k_dz = beta*Dz - Kz;
k_d = sqrt(k_dx*k_dx + k_dy*k_dy + k_dz*k_dz);

fudge_dir = DxA*DxA + DyA*DyA + DzA*DzA - .25;     { need to fudge it? }
ddx = if(fudge_dir, DxA, k_dx/k_d);
ddy = if(fudge_dir, DyA, k_dy/k_d);
ddz = if(fudge_dir, DzA, k_dz/k_d);

            { Hologram efficiency }
```

```
l5 = Kx*Dz - Dx*Kz; m5 = -Dy*Kz; n5 = -Kx*Dy;
Q = sqrt(m5*m5 + l5*l5 + n5*n5);
lpar = (l5*Dz-n5*Dy)/Q; mpar = (m5*Dz + n5*Dx)/Q; npar = -(m5*Dy + l5*Dx)/Q;
a_xPx = m5/Q; a_xPy = -l5/Q; a_xPz = -n5/Q;
t3 = sqrt(m5*m5 + l5*l5);
a_yPx = -l5/t3; a_yPy = -m5/t3; a_yPz : 0;
t4 = Q*t3;
a_zPx = -m5*n5/t4; a_zPy = l5*n5/t4; a_zPz = -(m5*m5 + l5*l5)/t4;
t5 = sqrt(1 + n5*n5/(l5*l5+m5*m5));
t_eff = t_h * t5;
Ci = abs(Dx*a_zPx + Dy*a_zPy + Dz*a_zPz);  { abs(x) is desparate measure }
Ck = -Kz/K * t5;
Cd = (beta*Ci - K*Ck) / beta;
xi = upsilon/(2*Cd);
upsilon = (beta*beta - k_d*k_d)/(2*beta);
nu = chi/sqrt(Ci*Cd);
eta_perp = nu*nu/(xi*xi + nu*nu) * sq(sin(sqrt(xi*xi+nu*nu)*t_eff));
t1 = sq(nu*(Dx*ddx+Dy*ddy+Dz*ddz));
eta_par = t1/(xi*xi + t1)*sq(sin(sqrt(xi*xi + t1)*t_eff));
           { Closed-form solution }
Sin_ti = if(.999999-Dz*Dz, sqrt(1-Dz*Dz), .001);
cos_pi = Dx/Sin_ti; sin_pi = Dy/Sin_ti;
cos_2pi = cos_pi*cos_pi - sin_pi*sin_pi;
sin_2pi = 2*sin_pi*cos_pi;
tan_ti = Sqrt(1-Dz*Dz)/Dz;
B1 = 1 + .5*tan_ti*tan_ti;
w11 = a_xPx - a_xPz*tan_ti*cos_pi; w21 = a_xPy - a_xPz*tan_ti*sin_pi;
T11 = .5*(w11*w11 + w21*w21); T21 = .5*(w11*w11 - w21*w21); T31 = w11*w21;
F_perp = 2*(T21*cos_2pi + T31*sin_2pi)/(tan_ti*tan_ti);
w12 = lpar - npar*tan_ti*cos_pi; w22 = mpar - npar*tan_ti*sin_pi;
T12 = .5*(w12*w12 + w22*w22); T22 = .5*(w12*w12 - w22*w22); T32 = w12*w22;
F_par = 2*(T22*cos_2pi + T32*sin_2pi)/(tan_ti*tan_ti);
eta_avg = eta_perp*(F_perp + (T11 - F_perp*B1)*dot) +
        eta_par*(F_par + (T12 - F_par*B1)*dot);

           { Diffraction efficiency }
dc = trans * eta_avg;

           { Transmitted component }
tdx = Dx; tdy = Dy; tdz = Dz;
tc = trans * (1 - eta_avg)
```

diffractC.cal

This subroutine is the same as the diffract.cal, except that it computes an average diffraction direction and efficiency over a selected wavelength range, rather than a single, discrete wavelength.

```
{
    Diffraction equation for grating without diffuser.

    Grating surface is in the X-Y plane, with grating aligned
    along the Y axis (i.e. rays are bent in X by grating).

    Taken from formulas provided by Physical Optics Corporation.
    Contact Indra Tengara (310) 320-3088 or (909) 396-0333.

    Input parameters:

    A1      - average index of refraction
    A2, A3, A4  - X, Y, Z of grating vector (1/microns)
    A5      - thickness of grating (microns)
    A6      - index modulation magnitude
    A7      - color component (1=Red,2=Green,3=Blue,4=grey)

    Computed values:

    dc      - diffracted component coefficient
    ddx, ddy, ddz   - diffracted component direction
    tc      - transmitted component coefficient
    tdx, tdy, tdz   - transmitted component direction
}
```

```
WL0 = select(arg(7), .646, .513, .380, .380);  { starting wavelength }
WL1 = select(arg(7), .780, .646, .513, .780);  { ending wavelength }
NWL = if(arg(7)-3.5, 3, 1) * 25;       { number of wavelength steps }
WLS = (WL1-WL0)/NWL;           { wavelength step size }

           { hologram-specific parameters }
n_avg = arg(1);         { average index of refraction }
Kx = arg(2);            { X component of grating vector (1/microns) }
Ky {= arg(3)} : 0;      { Y component of grating vector (always zero) }
Kz = arg(4);            { Z component of grating vector }
t_h = arg(5);           { grating thickness (microns) }
n_1 = arg(6);           { index modulation }

           { average f(lambda) over sample wavelengths }
wlsum(f,l) = f(l) + if(WL1-l-FTINY, wlsum(f,l+WLS), 0);
avg(f) = wlsum(f, WL0) / (NWL+1);

           { Fresnel reflection coefficients }
dot = abs(Dz);
C2 = sqrt(1 - (1-dot*dot)/(n_avg*n_avg));
F2_perp = sq((1/dot - n_avg/C2)/(1/dot + n_avg/C2));
F2_par = sq((dot - n_avg*C2)/(dot + n_avg*C2));
refl = .5 * (F2_perp + F2_par);
trans = 1 - refl;

           { Wave variables and diffracted direction }
K = sqrt(Kx*Kx + Ky*Ky + Kz*Kz);
beta(l) = 2*PI/l*n_avg;
chi(l) = PI/l*n_1;
k_dx(l) = beta(l)*Dx - Kx;
k_dy(l) = beta(l)*Dy - Ky;
k_dz(l) = beta(l)*Dz - Kz;
k_dx_a = avg(k_dx);
k_dy_a = avg(k_dy);
k_dz_a = avg(k_dz);
k_d = sqrt(k_dx_a*k_dx_a + k_dy_a*k_dy_a + k_dz_a*k_dz_a);


fudge_dir = DxA*DxA + DyA*DyA + DzA*DzA - .25;     { need to fudge it? }
ddx = if(fudge_dir, DxA, k_dx_a/k_d);
ddy = if(fudge_dir, DyA, k_dy_a/k_d);
ddz = if(fudge_dir, DzA, k_dz_a/k_d);

           { Hologram efficiency }
l5 = Kx*Dz - Dx*Kz; m5 = -Dy*Kz; n5 = -Kx*Dy;
Q = sqrt(m5*m5 + l5*l5 + n5*n5);
lpar = (l5*Dz-n5*Dy)/Q; mpar = (m5*Dz + n5*Dx)/Q; npar = -(m5*Dy + l5*Dx)/Q;
a_xPx = m5/Q; a_xPy = -l5/Q; a_xPz = -n5/Q;
t3 = sqrt(m5*m5 + l5*l5);
a_yPx = -l5/t3; a_yPy = -m5/t3; a_yPz : 0;
t4 = Q*t3;
a_zPx = -m5*n5/t4; a_zPy = l5*n5/t4; a_zPz = -(m5*m5 + l5*l5)/t4;
t5 = sqrt(1 + n5*n5/(l5*l5+m5*m5));
t_eff = t_h * t5;
Ci = abs(Dx*a_zPx + Dy*a_zPy + Dz*a_zPz);  { abs(x) is desparate }
Ck = -Kz/K * t5;
Cd(l) = (beta(l)*Ci - K*Ck) / beta(l);
upsilon(l) = (sq(beta(l)) - k_d*k_d)/(2*beta(l));
xi(l) = upsilon(l)/(2*Cd(l));
nu(l) = chi(l)/sqrt(Ci*Cd(l));
eta_perp(l) = sq(nu(l))/(sq(xi(l)) + sq(nu(l))) *
        sq(sin(sqrt(sq(xi(l))+sq(nu(l)))*t_eff));
t1(l) = sq(nu(l)*(Dx*ddx+Dy*ddy+Dz*ddz));
eta_par(l) = t1(l)/(sq(xi(l)) + t1(l))*sq(sin(sqrt(sq(xi(l)) + t1(l))*t_eff));
           { Closed-form solution }
Sin_ti = if(.999999-Dz*Dz, sqrt(1-Dz*Dz), .001);
cos_pi = Dx/Sin_ti; sin_pi = Dy/Sin_ti;
cos_2pi = cos_pi*cos_pi - sin_pi*sin_pi;
sin_2pi = 2*sin_pi*cos_pi;
tan_ti = Sqrt(1-Dz*Dz)/Dz;
B1 = 1 + .5*tan_ti*tan_ti;
w11 = a_xPx - a_xPz*tan_ti*cos_pi; w21 = a_xPy - a_xPz*tan_ti*sin_pi;
T11 = .5*(w11*w11 + w21*w21); T21 = .5*(w11*w11 - w21*w21); T31 = w11*w21;
F_perp = 2*(T21*cos_2pi + T31*sin_2pi)/(tan_ti*tan_ti);
w12 = lpar - npar*tan_ti*cos_pi; w22 = mpar - npar*tan_ti*sin_pi;
T12 = .5*(w12*w12 + w22*w22); T22 = .5*(w12*w12 - w22*w22); T32 = w12*w22;
```

```
F_par = 2*(T22*cos_2pi + T32*sin_2pi)/(tan_ti*tan_ti);
eperpc = F_perp + (T11 - F_perp*B1)*dot;
eparc = F_par + (T12 - F_par*B1)*dot;
eta_avg_l(l) = eta_perp(l)*eperpc + eta_par(l)*eparc;
eta_avg = avg(eta_avg_l);

            { Diffraction efficiency }
dc = trans * eta_avg;

            { Transmitted component }
tdx = Dx; tdy = Dy; tdz = Dz;
tc = trans * (1 - eta_avg);
```

rayinit.cal

This subroutine computes the standard initialization file for the RADIANCE procedural input.

```
{ SCCSid "@(#)rayinit.cal 2.10 2/29/96 LBL" }

{
    Initialization file for Radiance.

    The following are predefined:

    Dx, Dy, Dz          - ray direction
    Nx, Ny, Nz          - surface normal
    Px, Py, Pz          - intersection point
    T               - distance from start
    Ts              - single ray (shadow) distance
    Rdot                - ray dot product
    S               - world scale
    Tx, Ty, Tz          - world origin
    Ix, Iy, Iz          - world i unit vector
    Jx, Jy, Jz          - world j unit vector
    Kx, Ky, Kz          - world k unit vector
    arg(n)              - real arguments, arg(0) is count

    For brdf functions, the following are also available:

    NxP, NyP, NzP           - perturbed surface normal
    RdotP               - perturbed ray dot product
    CrP, CgP, CbP           - perturbed material color

    For prism1 and prism2 types, the following are available:

    DxA, DyA, DzA           - direction to target light source

    Library functions:

    if(a, b, c)         - if a positive, return b, else c

    select(N, a1, a2, ..)       - return aN

    sqrt(x)             - square root function

    sin(x), cos(x), tan(x),
    asin(x), acos(x),
    atan(x), atan2(y,x)     - standard trig functions

    floor(x), ceil(x)       - g.l.b. & l.u.b.

    exp(x), log(x), log10(x)    - exponent and log functions

    erf(z), erfc(z)         - error functions

    rand(x)             - pseudo-random function (0 to 1)

    hermite(p0,p1,r0,r1,t)      - 1-dimensional hermite polynomial

    noise3(x,y,z), noise3a(x,y,z),
    noise3b(x,y,z), noise3c(x,y,z)  - noise function with gradient (-1 to 1)

    fnoise3(x,y,z)          - fractal noise function (-1 to 1)
```

```
}


            { Backward compatibility }
AC = arg(0);
A1 = arg(1); A2 = arg(2); A3 = arg(3); A4 = arg(4); A5 = arg(5);
A6 = arg(6); A7 = arg(7); A8 = arg(8); A9 = arg(9); A10 = arg(10);

            { Forward compatibility (?) }
D(i) = select(i, Dx, Dy, Dz);
N(i) = select(i, Nx, Ny, Nz);
P(i) = select(i, Px, Py, Pz);
noise3d(i,x,y,z) = select(i, noise3a(x,y,z), noise3b(x,y,z), noise3c(x,y,z));

            { More robust versions of library functions }
bound(a,x,b) : if(a-x, a, if(x-b, b, x));
Acos(x) : acos(bound(-1,x,1));
Asin(x) : asin(bound(-1,x,1));
Atan2(y,x) : if(x*x+y*y, atan2(y,x), 0);
Exp(x) : if(-x-100, 0, exp(x));
Sqrt(x) : if(x, sqrt(x), 0);

            { Useful constants }
PI : 3.14159265358979323846;
DEGREE : PI/180;
FTINY : 1e-7;

            { Useful functions }
and(a,b) : if( a, b, a );
or(a,b) : if( a, a, b );
not(a) : if( a, -1, 1 );
abs(x) : if( x, x, -x );
sgn(x) : if( x, 1, if(-x, -1, 0) );
sq(x) : x*x;
max(a,b) : if( a-b, a, b );
min(a,b) : if( a-b, b, a );
inside(a,x,b) : and(x-a,b-x);
frac(x) : x - floor(x);
mod(n,d) : n - floor(n/d)*d;
tri(n,d) : abs( d - mod(n-d,2*d) );
linterp(t,p0,p1) : (1-t)*p0 + t*p1;

noop(v) = v;
clip(v) = bound(0,v,1);
noneg(v) = if(v,v,0);
red(r,g,b) = if(r,r,0);
green(r,g,b) = if(g,g,0);
blue(r,g,b) = if(b,b,0);
grey(r,g,b) = noneg(.265074126*r + .670114631*g + .064811243*b);
clip_r(r,g,b) = bound(0,r,1);
clip_g(r,g,b) = bound(0,g,1);
clip_b(r,g,b) = bound(0,b,1);
clipgrey(r,g,b) = min(grey(r,g,b),1);

dot(v1,v2) : v1(1)*v2(1) + v1(2)*v2(2) + v1(3)*v2(3);
cross(i,v1,v2) : select(i,  v1(2)*v2(3) - v1(3)*v2(2),
                v1(3)*v2(1) - v1(1)*v2(3),
                v1(1)*v2(2) - v1(2)*v2(1));

fade(near_val,far_val,dist) = far_val +
        if (16-dist, (near_val-far_val)/(1+dist*dist), 0);

bezier(p1, p2, p3, p4, t) =     p1 * (1+t*(-3+t*(3-t))) +
                p2 * 3*t*(1+t*(-2+t)) +
                p3 * 3*t*t*(1-t) +
                p4 * t*t*t ;

bspline(pp, p0, p1, pn, t) =    pp * (1/6+t*(-.5+t*(.5-1/6*t))) +
                p0 * (2/3+t*t*(-1+.5*t)) +
                p1 * (1/6+t*(.5+t*(.5-.5*t))) +
                pn * (1/6*t*t*t) ;

turbulence(x,y,z,s) = if( s-1.01, 0, abs(noise3(x/s,y/s,z/s)*s) +
                        turbulence(x,y,z,2*s) );

turbulencea(x,y,z,s) = if( s-1.01, 0,
```

```
            sgn(noise3(x/s,y/s,z/s))*noise3a(x/s,y/s,z/s) +
            turbulencea(x,y,z,2*s) );
turbulenceb(x,y,z,s) = if( s-1.01, 0,
            sgn(noise3(x/s,y/s,z/s))*noise3b(x/s,y/s,z/s) +
            turbulenceb(x,y,z,2*s) );
turbulencec(x,y,z,s) = if( s-1.01, 0,
            sgn(noise3(x/s,y/s,z/s))*noise3c(x/s,y/s,z/s) +
            turbulencec(x,y,z,2*s) );

            { Normal distribution from uniform range (0,1) }

un2`private(t) : t - (2.515517+t*(.802853+t*.010328))/
        (1+t*(1.432788+t*(.189269+t*.001308))) ;
un1`private(p) : un2`private(sqrt(-2*log(p))) ;

unif2norm(p) : if( .5-p, -un1`private(p), un1`private(1-p) ) ;

nrand(x) = unif2norm(rand(x));

            { Local (u,v) coordinates for planar surfaces }
crosslen`private = Nx*Nx + Ny*Ny;
            { U is distance from projected Z-axis }
U = if( crosslen`private - FTINY,
        (Py*Nx - Px*Ny)/crosslen`private,
        Px);
            { V is defined so that N = U x V }
V = if( crosslen`private - FTINY,
        Pz - Nz*(Px*Nx + Py*Ny)/crosslen`private,
        Py);
```

hologram design

The design of the holographic glazings was determined using the following code.

```
{
        Design a holographic glazing.

        10/28/96     Greg Ward
}

D : PI/180;     { radians per degree }
WL : .555;      { design wavelength (microns) }
n : 1.5;        { mean index of refraction for substrate }

{ Input ti and td in degrees:
        ti      - incident angle above horizontal
        td      - diffracted angle above horizontal
}

K : 2*PI*n/WL;

{ Output is computed below, zsgn, Kx and Kz:
        Kx      - X-component of gradient vector (always positive)
        Ky      - Y-component of gradient vector (always zero)
        Kz      - Z-component of gradient vector (always positive)
        zsgn    - 1 if Z-axis points into room, -1 if it points out of room
}

zsgn = if(ti-td, -1, 1);        { reverse Z axis? }

Kx = K * (sin(ti*D) + sin(td*D));
Ky : 0;         { always zero }
Kz = K*zsgn * (cos(ti*D) - cos(td*D));
```

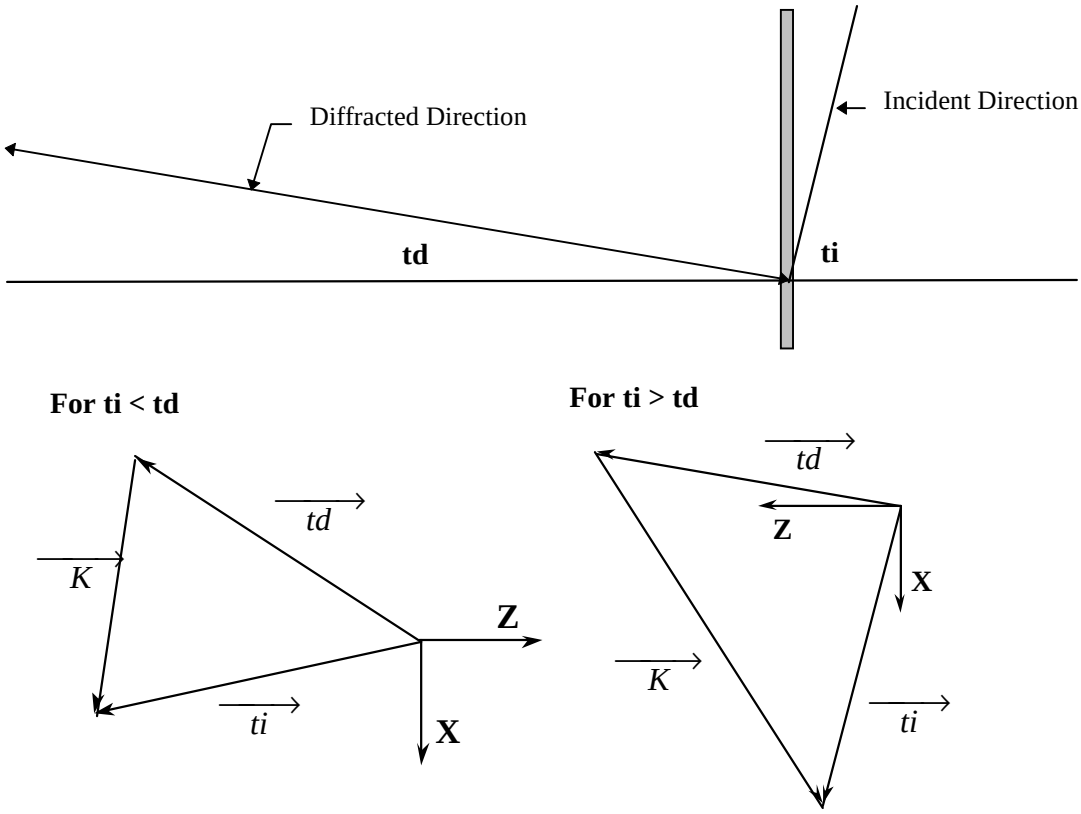

By providing the desired **ti** and **td,** the resulting **Kx** and **Kz** for the simulated wavelength **(.555 microns)** of light are then input into the Radiance description of the glazing sample, as shown below:

```
# Holographic glazing with 50° acceptance and 55.7° diffraction.
void prism2 holo3_green
13 dc ddx ddy ddz tc tdx tdy tdz diffract.cal -rz 90 -rx -90
0
7 1.5 18.25 0 5.23 10 .029 .555
#7 avg_index_of_refraction kx ky kz thick index_modulation_magnitude wavelength_center
holo3_green polygon window
0  0
12
        21      31.25    7
        21      31.25    9
        1       31.25    9
        1       31.25    7
```